# Aluminium Coated Single- and Multi-Mode Fibers for High Temperatures and High Doses

H. Boiron, A. Morana, *Member, IEEE,* A. Steib, R. Pouyet, A. Monteville, P. Guitton, S. Chaton, G. Mélin, T. Robin, and S. Girard, *Senior Member, IEEE*

***Abstract*—We investigate the combined temperature (25°C and 200°C) and radiation effects (up to 1 MGy of 40 keV X-rays) on the radiation-induced attenuation levels of fluorine-doped optical fibers with Al coatings.**

***Index Terms*—Aluminum coating, optical fiber, radiation induced attenuation.**

## I. Introduction

In numerous contexts, extreme environments pose significant challenges for instrumentation design. Such environments include not only extreme temperatures, but also sometimes high radiation levels. Creating instruments or systems that can reliably function under these combined constraints represents a considerable technological challenge, limiting the range of feasible solutions.

Over the past several decades, silica-based optical fibers have proven to be a highly attractive option for instrumentation in such demanding fields. Their small form factor, resilience to electromagnetic interference, cost-effectiveness make them key technologies for high-bandwidth data links or long-distance distributed sensors able to operate in severe constraints [1]. When deploying optical fibers in such challenging environments, it is essential to carefully choose their chemical composition. Indeed, the vulnerability of optical fibers, usually defined by their radiation-induced attenuation (RIA) level, strongly depends on the dopants and impurities incorporated within their silica-based core and cladding [2]. In application scenarios associated with very high total ionizing doses (TID), typically several MGy, optical fibers with either fluorine-doped core or pure silica core (PSC) and fluorine-doped claddings have already demonstrated the highest radiation tolerance in terms of RIA at Telecom wavelengths. However, their radiation vulnerability levels vary across the entire spectral range. In the ultraviolet (UV) [3] and visible (VIS) [4] domains, various point defects, having absorption bands peaking in these domains, are created by radiation through ionization, leading to significant RIA levels. Furthermore, due to the physics of those point defects, the RIA is strongly dependent on wavelength, dose, dose rate or temperature. At high total doses, typically above 300 kGy, RIA at 1550 nm tends to be significantly higher than at 1310 nm [5]. Consequently, there exists a spectral window between 1 µm and 1.2 µm where PSC fibers exhibit the lowest transmission degradation at very high doses [6], corresponding to their highest radiation tolerance. Naturally, this has led many applications to focus on this wavelength range, such as temperature sensing using Raman Distributed Temperature Sensing (RDTS) techniques [7], [8].

In extreme environments, RDTS measurements can be impacted by both radiation or $H_2$ diffusion through differential losses (due to RIA or hydrogen-related losses) between the Stokes and anti-Stokes signals at the basis of the temperature estimation [7], [9]. System-level solutions have been developed to partially mitigate these errors, such as employing double-ended RDTS configurations [10] or solving it by using dual-laser systems [11], [12]. Although such system-level improvements are essential to ensure the sensing performance, they cannot replace the careful selection of an optical fiber intrinsically resistant to both radiation exposure and hydrogen loading. Within the framework of the 3F2E [13] project, Exail and Photonics Bretagne therefore developed aluminum-coated optical fibers, including a single-mode (RAD-SM) fiber optimized for operation at 1064 nm and a multimode graded-index (RAD-MMGI) fiber. The single-mode fiber (SMF) consists of a pure silica core surrounded by a fluorine-doped cladding, whereas the multimode fiber employs a fluorine-graded refractive index profile. In addition to an optimized chemical composition designed to enhance radiation resistance, the use of an aluminum coating ensures hermetic sealing of the fiber, effectively preventing hydrogen diffusion [14] and allowing to use the fiber at high temperatures (up to $400\,°C$ versus $80\,°C$ for a standard acrylate coated fiber).

In order to evaluate both the radiation tolerance of these aluminum-coated fibers and the temperature dependence of their RIA levels and kinetics, irradiation experiments were carried out at LabH6 - a joint laboratory between Exail and the Hubert Curien Laboratory at Jean Monnet University in Saint-Étienne - using the LABHX X-ray irradiation machine [15]. After introducing in more details the tested fibers and experimental setups, we present the initial characterization results of the radiation response of the RAD-SM optical fiber at both $25\,°C$ and $200\,°C$, subjected to a total ionizing dose of $1\,MGy$ at a dose rate of $5\,Gy(SiO_2)/s$ of X-rays. In this abstract, only the results related to the RAD-SM fiber are presented to respect the page limit. However, the same study will be presented at the conference for the RAD-MMGI fiber. Lastly, we will conclude by addressing the ongoing and future

This work was supported by the 3F2E project for "French Fiber Field for Extreme Environment", funded by the post-pandemic France Economic Stimulus Plan "Relaunch France" aimed at supporting investments and reinforcing the capabilities of the French nuclear industry.

H. Boiron, G. Mélin, A. Steib, P. Guitton, S. Chaton and T. Robin are with Exail, 22300 Lannion, France. (e-mail: hugo.boiron@exail.com).

A. Morana, and S. Girard are with Laboratoire Hubert Curien, Université Jean Monnet, 42000 Saint-Étienne, France (e-mail: sylvain.girard@univ-st-etienne.fr). S. Girard is also with Institut Universitaire de France (IUF), Paris, France

R. Pouyet and A. Monteville are with Photonics Bretagne, 22300 Lannion, France (e-mail: rpouyet@photonics-bretagne.com).

experiments that will be presented during the conference and in the final paper.

## II. Material and Method

This section describes the opto-geometric characteristics of the tested optical fibers. Subsequently, we will discuss the impact of having an Al coating on the dose deposition within the fiber core for photons of varying energy. Finally, we present our experimental procedure for the radiation tests.

### A. Aluminum-coated RAD-SM and RAD-MMGI optical fiber

The aluminium-coated RAD-SM fiber, IXF-RAD-SM-1060-014-AL, has a numerical aperture of 0.14 and a cut-off wavelength below $900\,nm$ in order to offer single mode propagation at $1064\,nm$. Its cladding diameter is of $125\,\mu m$ and the core diameter of $4.5\,\mu m$. The coating has a thickness of $21 \pm 3\,\mu m$ with a density of $2.7\,g/cm^3$. Details of the RAD-MMGI fiber will be provided for the final paper.

### B. Experimental setup

The experimental setup was designed to enable the spectral characterization of RIA in the RAD-SM fiber. In order to provide the most comprehensive understanding possible, measurements were performed from 400 nm to 1200 nm. To achieve this, two experimental benches were implemented: one dedicated to the visible range using either a QE Pro or a QE65000 spectrometer from Ocean Optics, and the other covering the near-infrared region using an NIR512 spectrometer from the same manufacturer. In all case, illumination was provided by a DH-2000-BAL broadband light source, with the deuterium lamp activated only for measurements in the visible spectral range. The used transport fibers are of the same type than the fiber under test to ensure low losses at the splices and stable modal propagation. These transport fibers were shielded and therefore not irradiated. To ensure sample uniformity, the fiber was arranged as a single-layer. Measurements in the VIS were performed using 5 m long fiber samples, whereas near-IR measurements were carried out with 50 m long samples. The spatial uniformity of the radiation flux over the entire sample was assessed by measuring the dose rate at four cardinal positions along the coil using a calibrated PTW23344 ionization chamber. A dose-rate variation below 10 % was observed. The single-layer coil was subsequently positioned on a temperature-controlled heating plate set either to 25 °C or 200°C, with a temperature uncertainty of $\pm 1\,°C$. Thermal equilibrium was maintained for at least one hour before starting the irradiation.

Irradiations were performed using one of the X-ray machines from the PETRA platform of the Hubert Curien Laboratory, whose technical specifications are described in detail in [15]. The irradiators were operated at 100 kV, corresponding to X-rays with mean energy fluence of 40 keV. Previous simulation studies have demonstrated the influence of the aluminum coating on X-ray dose deposition within the fiber core, this has been taken into account in this work [16]. By adjusting the electron tube current of the irradiator, the dose rate was therefore set to 5 $Gy/s$.

## III. Processing and Results

This section presents a part of the experimental study conducted at 25 $°C$ and 200 $°C$ with a dose rate of 5 $Gy/s$, up to a TID of 1 $MGy$, on the RAD-SM fiber.

### A. Signal Processing

The visible and IR spectrometer records the signal transmitted ($I(\lambda, t)$) by the source throughout the experiment sample with a 1 $s$ period. The RIA, for a sample of length L is then calculated using the following formula:

$$RIA(\lambda, t) = -\frac{10}{L} \times \log_{10}\left(\frac{I(\lambda, t) - I_{Noise(\lambda)}}{I_{Ref}(\lambda) - I_{Noise(\lambda)}}\right) \qquad (1)$$

where $\lambda$ denotes the wavelength, $t$ the measurement time, $I_{Noise}$ the background noise (both electronical and optical) and $I_{Ref}$ the signal intensity measured prior starting the irradiation.

### B. Visible Domain

The following section presents the results obtained in the VIS range. Additional measurements will be performed and included for the conference. Fig. *1* shows a two-dimensional mapping of the visible RIA of the RAD-SM fiber as a function of both the dose and the wavelength during irradiation up to 1 MGy at 25°C (upper graph) and 200°C (lower graph).

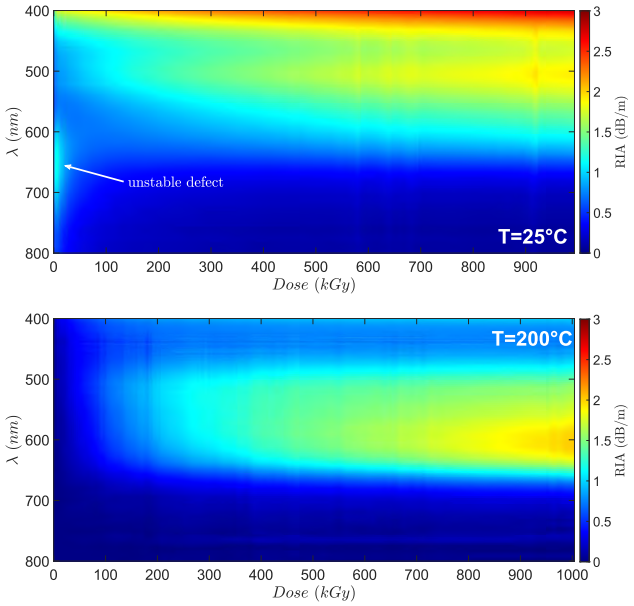


Fig. 1. 2D mapping of the visible RIA of the RAD-SM fiber as a function of both accumulated dose and wavelength during irradiation: 5 $Gy/s$ up to 1 $MGy$ at 25 $°C$ (upper graph) and 200 $°C$ (lower graph)

First, a transient RIA contribution from an unstable defect can be observed at the beginning of the measurements performed at 25 °C around 660 nm, which may correspond to the signature of a variant of self-trapped holes (STHs) [2]. Their known temperature instability could explain that they are not observed under irradiation at 200 °C. Fig. *1* also highlights the presence of a strong absorption band located in the UV region at the lowest temperature, whose absorption tail significantly impacts the transmission at 400 nm. This UV band is also present at 200 °C, although with a lower relative contribution to the RIA. Finally, the RIA spectra at the maximal dose differ at the two temperatures as better highlighted in Fig. 2, which

also presents the RIA spectra measured after 1 h of recovery at the irradiation temperature.

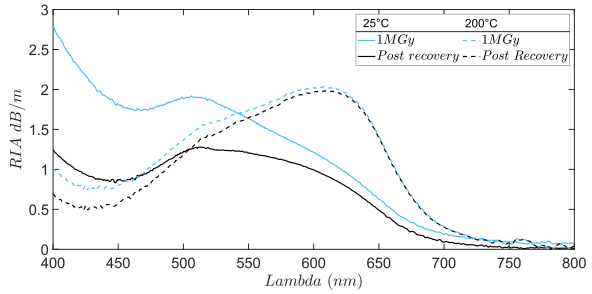


Fig. 2. RAD-SM RIA spectra measured at 1 MGy (5 Gy/s) and after 1 h of recovery at the irradiation temperature.

Fig. 2 therefore highlights the temperature dependence of the RIA in the RAD-SM fiber. Two defects can be visually identified, whose relative contributions to the total RIA vary with temperature. The first appears to absorb around 630 nm, which may correspond to the signature of non-bridging oxygen hole centers (NBOHCs, 1.97 eV [17]), whereas the second seems to be located near 505 nm and does not readily match any well-identified defect at first glance. A significant recovery can also be observed at shorter wavelengths, highlighting the instability of UV-absorbing defects regardless of the irradiation temperature. The unidentified band centered around 505 nm also exhibits partial recovery at both temperatures, whereas the NBOHC-related absorption appears comparatively stable. A complete spectral decomposition will be proposed for the conference, together with a detailed analysis of the kinetics of each defect throughout irradiation, notably building upon the work described in [18].

### C. *Near-Infrared Domain*

The analysis performed in the visible spectral range provides valuable insight into the physical mechanisms and defects involved. The following section therefore presents the results obtained in the infrared region, limited to $1200\,nm$, beyond which the optical losses of the as-drawn fiber strongly increase due to its cut-off wavelength.

Fig. *3* shows a two-dimensional mapping of the infrared RIA of the RAD-SM fiber as a function of both the dose and wavelength during irradiation at a dose rate of $5\,Gy/s$ up to $1\,MGy$ at $25\,°C$ (upper graph) and $200\,°C$ (lower graph). It should be noted that, unlike Fig. 2, the RIA is expressed here in dB/km. First, it should be recalled that both fibers were specifically designed to operate preferentially around $1064\,nm$. At this particular wavelength, the RIA remains below $20\,dB/km$ at $25\,°C$ and even below $10\,dB/km$ at $200\,°C$, demonstrating the excellent radiation resistance of these fibers at MGy dose level. Within the measured spectral range, Fig. *3* reveals the presence, at $25°C$, of a transient defect strongly absorbing in the visible range, whose tail is still observable. This may correspond to the contribution from the metastable $STH_2$ centers $(1.63\,eV)$ [2]. The amplitude of this defect, as well as its evolution throughout irradiation, is expected to strongly depend on the dose rate and be favored at high dose rates as the one of our work. This defect is absent at $200\,°C$.

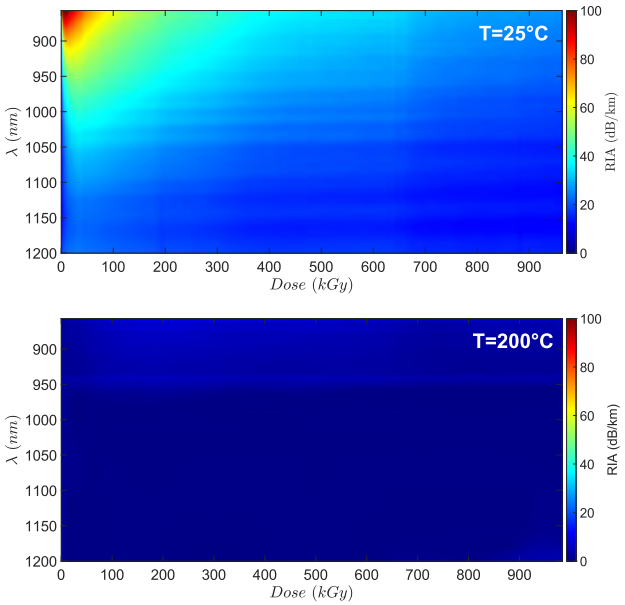


Fig. 3. 2D mapping of the infrared RIA of the RAD-SM fiber as a function of both dose and wavelength during irradiation: 5 Gy/s up to 1 MGy at 25°C (upper graph) and 200°C (lower graph).

More generally, Fig. *4* shows that, after 1 hour of recovery, the RIA converges toward similar levels independently of the irradiation temperature. This indicates that, at these wavelengths, the RIA is predominantly composed of metastable defects. Increasing the temperature accelerates their recombination during the irradiation, suggesting that the RIA response may also strongly depend on the dose rate.

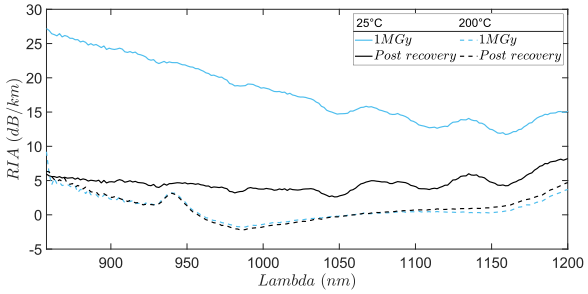


Fig. 4. RAD-SM infrared spectral RIA measured at the end of irradiation and after 1 h of recovery at the irradiation temperature.

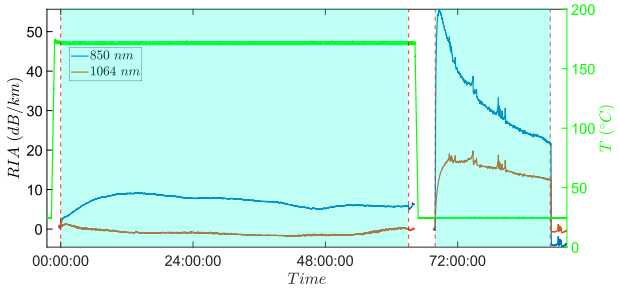


Fig. 5. Temporal evolution of the RIA at two wavelengths ($850\,nm$ and $1064\,nm$) during two successive irradiations: the first at $200\,°C$ and the second at $25\,°C$, both at $5\,Gy/s$.7

It is important to note that the recombination of these defects does not imply their complete annealing. One way to observe this effect is illustrated in Fig. 5 that gives the temporal evolution of the RIA at $850\,nm$ and $1064\,nm$ during two

successive irradiations: the first at $200\ °C$ and the second at $25\ °C$. Irradiation runs were performed at $5\ Gy/s$, indicated by the blue-shaded regions, while the right-hand y-axis displays the temperature evolution measured at the sample. To simplify data analysis and minimize the influence of temperature-dependent guiding effects and sample packaging, a reference RIA measurement was taken before each irradiation run, once the target temperature(s) had been stabilized. Fig. 5 further confirms that the RIA remains negligible at both wavelengths throughout irradiation at 200 °C. However, during the second irradiation performed at 25 °C, a significant increase in RIA can be observed, exhibiting a temporal evolution characteristic of metastable defect formation. We will show during the conference that the dynamics of this second irradiation are similar to those observed during a first irradiation at 25 °C, as presented in Fig. 3, although with a reduced amplitude. This means that the high dose pre-irradiation at 200°C does not fully eliminate the precursor sites at the origin of the defects causing the transient losses at room temperature.

## IV. Conclusion & Perspectives

This work investigated the radiation response of an aluminum-coated PSC single-mode (RAD-SM) fiber under combined high-dose (up to 1 MGy), elevated-temperature (25 °C and 200 °C), and X-ray irradiation conditions at 5 Gy/s. A pronounced temperature dependence of RIA was observed. In the visible range, the defect population and its spectral distribution strongly evolve with temperature. The spectral decomposition is not yet fully understood, particularly due to the presence of an unknown absorption band centred around 505 nm. This aspect will be further investigated and discussed in the final paper. In the near infrared region around 1064 nm, RIA is largely governed by metastable defects whose steady-state concentration results from the balance between generation and thermally activated recombination. Successive irradiations performed at different temperatures show that recombination does not necessarily imply complete recovery, and that metastable defects can still be generated even after a prior irradiation.

Future work will complete the spectral decomposition of the induced absorption bands and provide a detailed comparison between RAD-SM and RAD-MMGI fibers. Preliminary results on the RAD-MMGI fiber indicate comparable behaviour. Additional measurements at an intermediate temperature are planned to refine the understanding of recombination regimes.

## References


[1] S. Ma *et al.*, « Optical Fiber Sensors for High-Temperature Monitoring: A Review », *Sensors*, vol. 22, nº 15, p. 5722, juill. 2022, doi: 10.3390/s22155722.

[2] S. Girard *et al.*, « Overview of radiation induced point defects in silica-based optical fibers », *Rev. Phys.*, vol. 4, p. 100032, nov. 2019, doi: 10.1016/j.revip.2019.100032.

[3] H. Boiron *et al.*, « Radiation Induced Attenuation of Space-Grade Polarization-Maintaining Optical Fibers in the UV–Visible Domains », *Phys. Status Solidi A*, vol. 223, nº 2, p. e202500609, janv. 2026, doi: 10.1002/pssa.202500609.

[4] P. Borgermans et B. Brichard, « Kinetic models and spectral dependencies of the radiation-induced attenuation in pure silica fibers », *IEEE Trans. Nucl. Sci.*, vol. 49, nº 3, Art. nº 3, juin 2002, doi: 10.1109/TNS.2002.1039680.

[5] E. Shafir *et al.*, « Performance of an F-Doped Fiber Under Very High Ionizing Radiation Exposures », *IEEE Trans. Nucl. Sci.*, vol. 69, nº 12, Art. nº 12, déc. 2022, doi: 10.1109/TNS.2022.3224400.

[6] J. Blanc *et al.*, « Characterization of Radiation-Resistant Multimode Optical Fibers for Large-Scale Procurement », *IEEE Trans. Nucl. Sci.*, vol. 68, nº 7, p. 1407-1413, juill. 2021, doi: 10.1109/TNS.2021.3074633.

[7] F. B. H. Jensen, E. Takada, M. Nakazawa, T. Kakuta, et S. Yamamoto, « Consequences of radiation effects on pure-silica-core optical fibers used for Raman-scattering-based temperature measurements », *IEEE Trans. Nucl. Sci.*, vol. 45, nº 1, p. 50-58, févr. 1998, doi: 10.1109/23.659554.

[8] M. Agoyan, G. Cheymol, F. Martin, C. Destouches, A. Boukenter, et S. Girard, « In-core Gamma and Neutron Irradiation of Optical Materials used in the Design of an Optical Sensor for Pressurized Water Research Reactor », *IEEE Trans. Nucl. Sci.*, p. 1-1, 2026, doi: 10.1109/TNS.2026.3662197.

[9] C. Cangialosi *et al.*, « Hydrogen and radiation induced effects on performances of Raman fiber-based temperature sensors », présenté à OFS2014 23rd International Conference on Optical Fiber Sensors, J. M. López-Higuera, J. D. C. Jones, M. López-Amo, et J. L. Santos, Éd., Santander, Spain, juin 2014, p. 91576U. doi: 10.1117/12.2059628.

[10] A. F. Fernandez *et al.*, « Radiation-tolerant Raman distributed temperature monitoring system for large nuclear infrastructures », *IEEE Trans. Nucl. Sci.*, vol. 52, nº 6, p. 2689-2694, déc. 2005, doi: 10.1109/TNS.2005.860736.

[11] D. Di Francesca *et al.*, « Radiation Hardened Architecture of a Single-Ended Raman-Based Distributed Temperature Sensor », *IEEE Trans. Nucl. Sci.*, vol. 64, nº 1, p. 54-60, janv. 2017, doi: 10.1109/TNS.2016.2631539.

[12] A. Morana *et al.*, « Performances of Radiation-Hardened Single-Ended Raman Distributed Temperature Sensors Using Commercially Available Fibers », *IEEE Trans. Nucl. Sci.*, vol. 67, nº 1, p. 305-311, janv. 2020, doi: 10.1109/TNS.2019.2954586.

[13] « Aluminum-coated optical fibers in the nuclear field », Exail. Consulté le: 27 mars 2026. [En ligne]. Disponible sur: https://www.exail.com/news/enhancing-the-adoption-of-aluminum-coated-optical-fibers-in-the-nuclear-field

[14] J. Stone, « Interactions of hydrogen and deuterium with silica optical fibers: A review », *J. Light. Technol.*, vol. 5, nº 5, p. 712-733, 1987, doi: 10.1109/JLT.1987.1075562.

[15] A. Meyer, D. Lambert, A. Morana, P. Paillet, A. Boukenter, et S. Girard, « Simulation and Optimization of Optical Fiber Irradiation with X-rays at Different Energies », *Radiation*, vol. 3, nº 1, p. 58-74, mars 2023, doi: 10.3390/radiation3010006.

[16] H. Boiron *et al.*, « Impact of Coating Type on the Radiation Response of Germanosilicate Optical Fibers at High Temperatures », in *2024 24th European Conference on Radiation and Its Effects on Components and Systems (RADECS)*, Maspalomas, Spain: IEEE, sept. 2024, p. 1-4. doi: 10.1109/RADECS61970.2024.11298621.

[17] S. Girard *et al.*, « Overview of Radiation Effects on Silica-Based Optical Fibers and Fiber Sensors », *IEEE Trans. Nucl. Sci.*, vol. 72, nº 4, p. 982-1020, avr. 2025, doi: 10.1109/TNS.2024.3511455.

[18] C. Campanella *et al.*, « Radiation Effects on Pure-Silica Multimode Optical Fibers in the Visible and Near-Infrared Domains: Influence of OH Groups », *Appl. Sci.*, vol. 11, nº 7, p. 2991, mars 2021, doi: 10.3390/app11072991.